Biomaterials 83 (2016) 294–307

Contents lists available at ScienceDirect

Biomaterials

journal homepage: www.elsevier.com/locate/biomaterials

Sonoprinting and the importance of microbubble loading for the ultrasound mediated cellular delivery of nanoparticles

Ine De Cock [a], Guillaume Lajoinie [b], Michel Versluis [b], Stefaan C. De Smedt [a, *, 1], Ine Lentacker [a, 1]

[a] Laboratory of General Biochemistry and Physical Pharmacy, Ghent Research Group on Nanomedicine, Faculty of Pharmaceutical Sciences, Ghent University, Ottergemsesteenweg 460, Ghent, Belgium
[b] Physics of Fluids Group, MESA+ Institute for Nanotechnology and MIRA Institute for Biomedical Technology and Technical Medicine, University of Twente, P.O. Box 217, 7500 AE, Enschede, The Netherlands

ARTICLE INFO

Article history:
Received 16 October 2015
Received in revised form
24 December 2015
Accepted 1 January 2016
Available online 6 January 2016

Keywords:
Ultrasound
Microbubbles
Drug delivery
Loaded microbubbles
Mechanisms

ABSTRACT

In the last years, research on ultrasound mediated drug delivery using microbubbles is vastly expanding. While some groups simply mix drugs and microbubbles (co-administration), other researchers have a major interest in the potential of drug-loaded microbubbles. However, today, little is known on the pros and cons of these two strategies. In this study we evaluated the delivery of nanoparticles (polystyrene nanospheres and mRNA-lipoplexes) to cells *in vitro*, in case the nanoparticles were mixed with unloaded microbubbles versus loaded onto the microbubbles. Flow cytometry experiments demonstrated that unloaded microbubbles did not enhance the cellular delivery of the nanospheres and mRNA-lipoplexes. However, upon loading the nanoparticles onto the microbubbles, their delivery to cells substantially improved. Real-time swept field confocal microscopy imaging of the microbubbles and cells during ultrasound radiation revealed that nanoparticle-loaded microbubbles directly deposited the nanoparticles in patches onto the cell membrane, a process that we termed 'sonoprinting'. This phenomenon resulted in the delivery of large amounts of nanoparticles to the cells and is suggested to be different from the creation of cell membrane pores and enhanced endocytosis, which have been reported before as mechanisms behind the improved delivery of drugs to cells by ultrasound.

1. Introduction

Ultrasound-based techniques show great potential to locally enhance drug delivery by permeabilizing cellular membranes [1]. Microbubbles, being micrometer-sized gas structures stabilized by a lipid, polymer or protein shell, lower the acoustic energy needed for these processes. In an ultrasonic field, microbubbles undergo volumetric oscillations, termed cavitation. Microbubble cavitation evokes biophysical effects on neighboring cells, leading to enhanced drug delivery [2]. These biophysical effects include (i) the oscillatory motion of the microbubble resulting in pushing and pulling on the cell membrane, (ii) translation of the microbubble by which it presses against the cell membrane and (iii) microstreaming in the fluid surrounding the microbubble, which generates shear stresses on cells. When high acoustic pressures are applied, microbubbles can implode which is accompanied with more violent biophysical effects such as (iv) shock wave formation and (v) microjetting. These microbubble-cell interactions have been reported to facilitate drug delivery by two mechanisms, i.e. the generation of cell membrane pores through which drugs can passively diffuse [3] and enhanced endocytosis [4]. In previous experiments, we demonstrated that the acoustic pressure strongly influences which uptake mechanism occurs: at low acoustic pressures endocytosis is enhanced, while higher acoustic pressures favor uptake via membrane pores [5]. However, it should be noted that in our previous experiments, as well as in most studies evaluating mechanisms of ultrasound mediated delivery, rather small fluorescent probes, e.g. propidium iodide [6], calcein [7], dextrans [4], with a size ranging from a few to tens of nanometers, were used. Moreover these probes were mixed with and not loaded onto

* Corresponding author. Laboratory of General Biochemistry and Physical Pharmacy, Ottergemsesteenweg 460, 9000, Ghent, Belgium.
E-mail addresses: Ine.DeCock@UGent.be (I. De Cock), Stefaan.DeSmedt@UGent.be (S.C. De Smedt).
[1] Both last authors contributed equally.

http://dx.doi.org/10.1016/j.biomaterials.2016.01.022
0142-9612/

the microbubbles during the experiments.

Meanwhile, an increasing number of researchers are exploring novel strategies to load microbubbles with drugs [8]. Although microbubbles can serve as vehicles for low molecular weight drugs, e.g. by dissolving them in an oil layer between the microbubble shell and core [9] or by incorporating them into the microbubble shell [10], loaded microbubbles are mainly designed to deliver larger molecules or nanoparticles. For example, by including positively charged compounds into the microbubble shell, negatively charged nucleic acids (e.g. pDNA, siRNA, mRNA) can be loaded electrostatically onto the microbubble [11]. Another technique consists in encapsulating the drug into nanoparticles, such as liposomes, and subsequently attaching the nanoparticles onto the microbubble shell, as reported by our group [12–14]. Several rationales are driving the design of these new constructs. Ultrasound itself already provides controlled delivery in (i) time, by monitoring the onset and duration of ultrasound, and (ii) space, by exposing only the target tissue to ultrasound. Drug-loaded microbubbles may further optimize ultrasound triggered drug delivery, since the drugs are assumed to be released only when the microbubbles are exposed to ultrasound. Hence, the drug concentration is expected to increase locally, while the non-exposed tissue is left unharmed. Especially cytotoxic drugs like chemotherapeutics could benefit from this approach [15,16]. Moreover, loading the drugs onto the microbubbles may protect them from degradation and clearance. This is of particular interest for nucleic acids, which rapidly degrade in biological fluids [17,18]. Interestingly, microbubbles are also clinically approved as contrast agents for diagnostic ultrasound imaging. Therefore, drug-loaded microbubbles show potential as theranostic tools, allowing both drug delivery and contrast for imaging [19,20].

The efficacy of drug-loaded microbubbles has been proven before in several studies, both *in vitro* and *in vivo* [1]. However, little attention is being paid to the mechanisms behind the drug delivery process with these constructs. It is assumed that upon ultrasound exposure, the microbubbles locally release their payload, while at the same time the microbubble cavitation enhances the uptake of the released drug. Eisenbrey et al. [21] reported that doxorubicin-loaded polymer microbubbles ruptured into 200–400 nm drug-containing fragments, which might be caused by sonic cracking of the shell [1]. Luan et al. [22] studied fluorescently labeled lipid-shelled microbubbles and recorded release of shell fragments by high-speed fluorescence imaging. These fragments were further transported by acoustic microstreaming. This so-called lipid shedding was already observed at pressures as low as 85 kPa, indicating that inertial collapse of the microbubble is not obligatory to induce release. Nevertheless, higher acoustic pressures increased the occurrence of shedding and extended the distance over which the lipids were expelled. Similar observations were seen with fluorescent liposomes attached to lipid-shelled microbubbles [23]. Lipid shedding was also investigated by Borden et al. [24]. They attributed the shedding process to acoustic dissolution of the microbubble, in which gas of the microbubble core is lost during oscillation. The accompanying reduction of surface area led to expulsion of the excess shell material. Both authors exclusively investigated the release of material from loaded microbubbles, though they did not study how the released molecules may be subsequently taken up cells, which is an equally essential step. As mentioned above, ultrasound mediated uptake is generally reported to occur via diffusion through cell membrane pores or via enhanced endocytosis. However, for microbubbles loaded with nanoparticles, it is unlikely that the delivery of the nanoparticles to the cells occurs by passive diffusion through the created cell membrane pores, to the same extent as occurs for smaller molecules.

In this study, we investigated the ultrasound induced delivery of nanoparticles to cells *in vitro* when the nanoparticles are loaded onto microbubbles and when they are physically mixed with the microbubbles (‘ unloaded microbubbles’ in Fig. 1, also termed ‘co-administration’ in *in vivo* situations). Especially, we aimed to understand how nanoparticle-loaded microbubbles are capable to deliver nanoparticles intracellularly. First, flow cytometry was performed to quantitatively measure the delivery of the nanoparticles to the cells. Second, real-time swept field confocal microscopy, recording events at a timescale of tens of milliseconds, was implemented to investigate the mechanisms behind the drug delivery processes. Two different types of nanoparticles were used: (i) fluorescent polystyrene nanospheres (20 nm and 100 nm) were chosen as model nanoparticles since they are highly fluorescent and therefore well-suited for imaging purposes; (ii) fluorescently labeled mRNA-lipoplexes (100 nm) were chosen as therapeutically more relevant nanoparticles since they are known as efficient cell transfection agents in several studies [25]. The loading of the nanoparticles to lipid-shelled microbubbles was achieved through biotin-avidin bridging (Fig. 1), as previously reported by our research group [14,15,25].

2. Materials and methods

2.1. Cell culture

Human melanoma cells (BLM cells) [26] were grown in culture flasks in a humidified atmosphere with 5% CO_2 at 37 °C. The culture medium was Dulbecco's Modified Eagle Medium with Nutrient Mixture F12 (Gibco, Merelbeke, Belgium), supplemented with 10% (v/v) fetal bovine serum (FBS) (Hyclone, Thermo Scientific, MA, USA), 20 U/mL penicillin-streptomycin (Gibco, Merelbeke, Belgium), 2 mM L-glutamine (Gibco, Merelbeke, Belgium) and

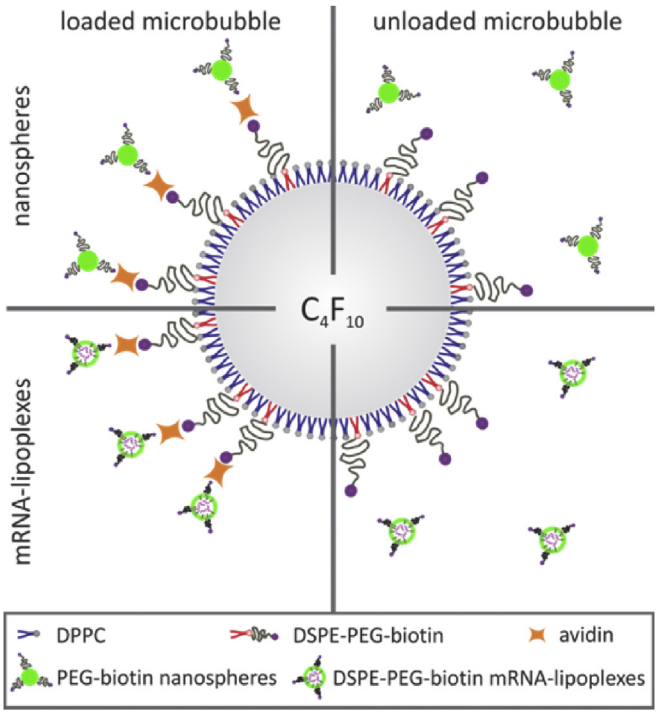

Fig. 1. Schematic representation of the microbubbles and nanoparticles. Fluorescent polystyrene nanospheres or fluorescent mRNA-lipoplexes were (left) loaded onto the microbubble lipid shell via biotin-avidin bridging, or (right) mixed with unloaded microbubbles.

10 mM HEPES (4-(2-hydroxyethyl)-1-piperazineethanesulfonic acid) (Sigma–Aldrich, Diegem, Belgium). One day before the experiment, cells were harvested by 0.05% trypsin-EDTA (ethylenediaminetetraacetic acid) (Gibco, Merelbeke, Belgium) and replated in Opticells™ (Nunc, Thermo Scientific, MA, USA). For flow cytometry experiments, cells were seeded at a density of 2×10^6 cells/mL, reaching confluency after 1 day. For microscopy experiments, a cell density of 1×10^6 cells/mL was used to obtain a sub-confluent monolayer.

2.2. Polystyrene nanospheres

Yellow-green fluorescent (excitation/emission: 505/515 nm) 20 nm and 100 nm carboxylate modified polystyrene Fluospheres® were purchased from Life Technologies (Merelbeke, Belgium). The nanospheres were covalently coated with polyethyleneglycol-biotin via amine-coupling as follows. 2 kDa biotin-PEG-amine (Creative PEGWorks, Winston Salem, NC, USA), N-(3-dimethylaminopropyl)-N′-ethylcarbodiimide hydrochloride (EDC) (Sigma–Aldrich), and N-hydroxysulfosuccinimide sodium salt (sulfo-NHS) (Sigma–Aldrich) were dissolved in HEPES Buffered Saline (HBS) (10 mM HEPES (Sigma–Aldrich), 150 mM NaCl (Sigma–Aldrich)) containing 3.4 mM EDTA (Merck, Overijse, Belgium), 0.005% Tween 20 (Sigma–Aldrich) and adjusted to pH 8. The nanospheres were added to this mixture to give final concentrations of 4 mg/mL EDC, 1.13 mg/mL Sulfo-NHS, 10 mg/mL biotin-PEG-amine and 1% nanospheres. The mixture was rotated overnight at room temperature. The 0.1 μm PEG-biotin nanospheres were purified by ultracentrifugation (Beckman L8-70M Ultracentrifuge, Beckman–Coulter, Brea, CA, USA) at 234,000 g for 45 min and resuspended in HBS to obtain a concentration of 2% solids. The 0.02 μm PEG-biotin nanospheres were purified using a Spectra/Por® dialysis membrane with a 300,000 MW cut-off (SpectrumLabs, Breda, The Netherlands). During the dialysis process, the nanosphere dispersion was diluted. Therefore, the concentration was determined by plotting a calibration curve based on known concentrations and measured fluorescence intensities (Envision Multilabel Plate Reader, Perkin Elmer, Waltham, MA, USA). The concentration was found to be 0.45% solids. The size and zeta potential of the nanospheres were measured in HEPES buffer (20 mM, pH 7.5) using a Zetasizer Nano (Malvern, Worcestershire, United Kingdom) and the particles were stored at 4 °C.

2.3. mRNA-lipoplexes

mRNA-lipoplexes were prepared by complexing cationic liposomes with mRNA, as described previously [20]. First, luciferase mRNA was produced by *in vitro* transcription from pBlue-Luc-A50 plasmids. The plasmids were purified using a QIAquick PCR purification kit (Qiagen, Venlo, The Netherlands) and linearized using Dra I restriction enzymes (Promega, Leiden, The Netherlands). Linearized plasmids were used as templates for the *in vitro* transcription reaction using the T7 mMessage mMachine kit (Ambion, Life Technologies, Ghent, Belgium). The resulting capped and polyadenylated mRNAs were purified by DNase I digestion, LiCl precipitation and washed with 70% ethanol. The mRNA concentration was determined by measuring the absorbance at 260 nm mRNA was stored in small aliquots at −80 °C at a concentration of 1 μg/μL. Subsequently, cationic liposomes were prepared and consisted of 42 mol% DOTAP (1,2-dioleoyl-3-trimethylammonium-propane), 42 mol% DOPE (1,2-dioleoyl-sn-glycero-3-phosphoethanolamine, both Avanti Polar Lipids), 15% DSPE-PEG_{3400}-biotin [1,2-distearoyl-sn-glycero-3-phosphoethanol-amine-N-[biotinyl(polyethyleneglycol)-3400] (Laysan Bio Inc, Arab, Alabama) and 1 mol% of the fluorescent lipid Cholesteryl-BODIPY® FL C12 (excitation/emission: 500/515 nm) (Life Technologies). The appropriate amounts of lipids (dissolved in chloroform) were transferred to a round-bottom flask, and the chloroform was evaporated under nitrogen. The resulting lipid film was hydrated in RNase-free water (Ambion) to obtain a final lipid concentration of 1 mg/mL. The obtained cationic liposomes were sonicated for 1 min in a bath sonicator (Branson Ultrasonics, Dansbury, USA) to reduce their size. Finally, 12 μg cationic liposomes were mixed with 10 μg mRNA and diluted to 100 μL with RNase-free water, obtaining mRNA-lipoplexes at a cationic lipid-to-mRNA charge (N/P) ratio of 8. The size and zeta potential of the lipoplexes were measured in HEPES buffer (20 mM, pH 7.5) using a Zetasizer Nano.

2.4. Microbubbles

Microbubbles composed of DPPC (1,2-dipalmitoyl-sn-glycero-3-phosphocholine) (Lipoid, Ludwigshafen, Germany) and DSPE-PEG_{3400}-biotin [1,2-distearoyl-sn-glycero-3-phosphoethanol-amine-N-[biotinyl(polyethyleneglycol)-3400] (Laysan Bio Inc, Arab, Alabama) were used. The DPPC/DSPE-PEG_{3400}-biotin molar ratio equaled 85:15 or 95:5 molar ratio when used with mRNA-lipoplexes or polystyrene nanospheres, respectively. For microscopy experiments, 0.5 mol% of the fluorescent lipid DiD (excitation/emission: 644/665 nm) (1,1′-Dioctadecyl-3,3,3′,3′-Tetramethylindodicarbocyanine, 4-Chlorobenzenesulfonate Salt, Life Technologies) was incorporated in the lipid shell. The microbubbles were prepared as described previously [5,25]. Appropriate amounts of the lipids dissolved in chloroform were transferred to a round-bottom flask. Subsequently, the chloroform was removed by evaporation. The obtained lipid film was dissolved in a 1:2:7 glycerol-propyleneglycol-water (Sigma–Aldrich, Diegem, Belgium) mixture, resulting in a solution with a lipid concentration of 0.75 mg/mL. Aliquots of this lipid solution were transferred into 2.5 mL chromatography vials, of which the headspace was filled with C_4F_{10} gas (F2 chemicals, Preston, UK). Finally, microbubbles were obtained by high speed shaking of the lipid solution for 15 s in a Capmix™ device (3 M-ESPE, Diegem, Belgium). To prepare drug-loaded constructs, microbubbles were subsequently coated with avidin. For this, the excess of lipids was first removed by centrifugation. Afterward, microbubbles were incubated for 5 min with avidin (Merck). The excess of avidin was again removed by centrifugation. Finally, microbubbles were resuspended in HEPES buffer (20 mM, pH 7.4) and incubated with the nanoparticles to obtain drug-loaded microbubbles. Unloaded microbubbles were similarly centrifuged twice, though without avidin incubation. The size and the concentration of the microbubbles in the dispersion were determined with a Multisizer™ 4 (Beckman Coulter, Brea, CA, USA).

2.5. Ultrasound equipment

Ultrasound pulses were generated by an arbitrary waveform generator (33220A, Agilent Technologies, Diegem, Belgium) and amplified by an amplifier (150A100B, Amplifier Research Benelux, Hazerswoude Dorp, The Netherlands). The amplified electrical signals were sent to an unfocused, single-element, 1 MHz center frequency transducer (A303S-SU, Olympus Industrial Benelux, Aartselaar, Belgium), which transmits the ultrasound waves. The transducer was mounted at the side of a water tank at a 45° angle and at 12 cm distance from the cell monolayer in the Opticell™. The water in the tank was degassed and heated at 37 °C. The Opticell™ chamber was marked with 9 exposure areas of 7 mm diameter. These areas correspond to regions homogeneously exposed to ultrasound, as calibrated with a needle hydrophone. The transmitted ultrasound signals were monitored with an oscilloscope (TDS 210, Tektronix, Bracknell, UK). A schematic representation of the setup is

depicted in Fig. 2. As described below, the ultrasound setup was mounted on a swept field confocal microscope for real-time confocal recordings.

2.6. Cellular uptake of nanoparticles analyzed by flow cytometry

50 μL of the microbubble suspension (±3 × 10^7 microbubbles) was pre-incubated with 100 μL mRNA-lipoplexes, 10 μL 100 nm or 15 μL 20 nm polystyrene nanospheres. Note that the 10 μL 100 nm and 15 μL 20 nm nanosphere dispersion showed the same total fluorescence. Subsequently, the microbubbles and nanoparticles were added to the cells in Opti-MEM® (Gibco, Merelbeke, Belgium). The Opticell™ was flipped to allow the microbubbles to rise against the cell monolayer and submerged in the water tank. Each of the 9 exposure areas marked on the Opticell™, as mentioned in Section 2.5., was radiated with ultrasound pulses with center frequency of 1 MHz, an acoustic pressure of 300 kPa, a pulse length of 1000 cycles and a repetition rate of 100 Hz for a total duration of 5 s. Following ultrasound exposure, the Opticells™ were placed back in the incubator for 30 min. Afterward, the exposure areas were cut out from the Opticell™, washed and transferred to a well plate. Control samples included (i) an 'untreated' sample, i.e. cells which were neither exposed to nanoparticles nor to ultrasound, (ii) a '4 °C' sample in which cells were pre-incubated on ice followed by a 30 min incubation with the nanoparticles on ice without ultrasound exposure, (iii) an 'endocytosis' sample in which cells were incubated with the nanoparticles at 37 °C without radiating them with ultrasound. Subsequently, cells were collected by trypsinization. In case of mRNA-lipoplexes, trypsinization was started at 4 h, 8 h, 16 h or 24 h after ultrasound exposure. Cells collected from three exposure areas were pooled in one tube, resulting in three samples per Opticell™. Before flow cytometric analysis, 0.04% trypan blue (Sigma–Aldrich) was added to one of the three samples. To evaluate cell viability, Calcein AM Red™ staining (excitation/emission maxima: 647/659 nm, Assay Biotech, Sunnyvale, CA, USA) was performed. Flow cytometric data were acquired using a FACSCalibur™ (BD, Erembodegem, Belgium) and analyzed using FlowJo™ software.

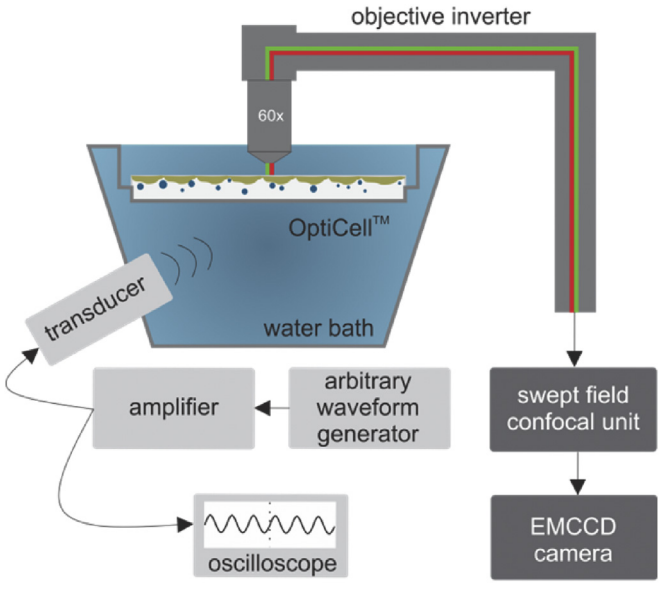

Fig. 2. Schematic representation of the ultrasound and swept field confocal microscope setup. The Opticell™ containing the cells, microbubbles and nanoparticles was submerged in a water bath. The ultrasound transducer was positioned below the Opticell™, while imaging occurred through a 60× water dipping lens placed on top by an objective inverter. Images were acquired by a swept field confocal unit and an EMCCD camera, operating at a frame rate of between 11 and 24 fps.

2.7. Real-time swept field confocal microscopy during ultrasound exposure

The cell membrane of BLM cells was labeled with 4 μg/mL CellMask™ Deep Red Plasma membrane Stain (excitation/emission maxima: 649/666 nm, Molecular Probes, Merelbeke, Belgium). 25 μL of DiD-labeled microbubble suspension (±1.5 × 10^7 microbubbles) was pre-incubated with 5 μL 100 nm polystyrene beads or 50 μL mRNA-lipoplexes and afterward added to the cells in Opti-MEM®. Cells were exposed to ultrasound pulses with a center frequency of 1 MHz, an acoustic pressure of 300 kPa, a pulse length of 1000 cycles and a repetition rate of 100 Hz for a total duration of 5 s. To record microbubble-cell interactions in real-time, the ultrasound setup was mounted on an Eclipse Ti inverted microscope (Nikon), equipped with an objective inverter (LSM TECH, Wellsville, PA, USA) and an NIR Apo 60× 1.0 NA water dipping lens (Nikon) (Fig. 2). The microscope was connected to a LiveScan™ swept field confocal unit (Nikon), allowing reasonably fast imaging (frame rate of 11–24 fps) while maintaining confocal resolution (slit size 35 μm). This confocal unit was equipped with a 488/647 nm dichroic mirror and a 505/585/685 nm Brightline® triple-band bandpass filter (Semrock, Rochester, NY, USA). Fluorophores were excited by a 488 nm and 640 nm laser (Monolithic Laser Combiner MLC 400B, Agilent Technologies, Diegem, Belgium). Images were acquired with the NIS Elements AR software using an EMCCD camera (iXon Ultra 897, Andor Technology, CT, USA). At least 35 recordings were acquired for each nanoparticle type. Recordings were analyzed with Image J.

2.8. Statistical analysis

Flow cytometry data are presented in column graphs as mean ± standard deviation (SD). Experiments were performed in threefold. One-way ANOVA tests with a Bonferroni multiple comparison test (GraphPad software, La Jolla, CA, USA) were performed to determine whether groups significantly differed from each other. The number of asterisks in the figures indicates the statistical significance as follows: *$p < 0.05$, **$p < 0.01$, ***$p < 0.001$.

3. Results

3.1. Characterization of nanoparticles and microbubbles

To load the microbubbles with nanoparticles, biotin-avidin bridging was used (Fig. 1). For this, DSPE-PEG-biotin functionalized lipids were incorporated in the microbubble shell. Likewise, DSPE-PEG-biotin was added to the mRNA-lipoplex formulation. The polystyrene nanospheres were covalently coated with PEG-biotin groups, as described in the materials and methods section. The PEG-coating was successful, since the zeta potential of the negatively charged nanospheres increased after PEGylation, indicating partial shielding of the charge by the polymer coating (Table 1). The size of the nanospheres slightly increased upon PEG-coating. Note that the 20 nm nanospheres (according to the provider) are rather 40 nm in diameter, even before coating. The mRNA-lipoplexes were approximately 100 nm in size and showed a neutral zeta potential due to the high PEGylation degree of 15 mol%. By adding avidin to the biotinylated microbubbles, the biotinylated nanoparticles were able to attach to the microbubble shell, as can be seen from the confocal images depicted in Fig. 3. In addition, the unloaded and loaded microbubbles were characterized by Coulter counter measurements (Fig. 3). The microbubble concentrations ranged

Table 1
Characterization of the nanoparticles.

	20 nm nanospheres		100 nm nanospheres		mRNA-lipoplexes
	−PEG[c]	+PEG[d]	−PEG[c]	+PEG[d]	+PEG
Size[a] ± SD (nm)	37 ± 1	42 ± 2	106 ± 2	134 ± 3	113 ± 3
PDI[b]	0.2	0.1	0.03	0.03	0.2
Zeta potential ± SD (mV)	−36 ± 20	−10 ± 8	−60 ± 16	−14 ± 5	−1 ± 4

[a] Hydrodynamic diameter (z-average).
[b] Polydispersity index.
[c] Purchased nanospheres.
[d] PEG-biotin modified nanospheres.

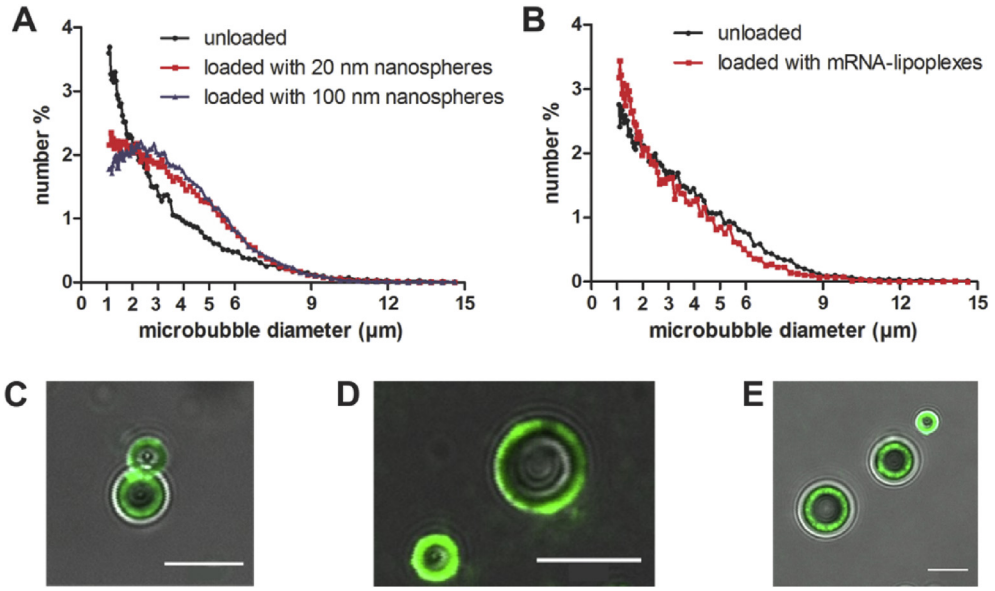

Fig. 3. Characterization of the microbubbles. Size distribution of (A) unloaded and nanosphere-loaded microbubbles, (B) unloaded and mRNA-lipoplex-loaded microbubbles, as determined by Coulter counter measurements. Overlays of transmission images and green fluorescent confocal images of (C) 20 nm nanosphere-loaded microbubbles, (D) 100 nm nanosphere-loaded microbubbles and (E) mRNA-lipoplex-loaded microbubbles. The white scale bars in the confocal images represent 5 μm.

between 3×10^8 and 8×10^8 microbubbles/mL. The mean diameter of the microbubbles ranged between 2.4 and 2.9 μm and did not change notably by loading them with nanospheres or mRNA-lipoplexes.

3.2. Cellular uptake of nanospheres with unloaded or loaded microbubbles

Flow cytometry was performed to quantitatively evaluate the cellular uptake of polystyrene nanospheres when mixed with or attached to lipid microbubbles and exposed to ultrasound (center frequency of 1 MHz, an acoustic pressure of 300 kPa, a pulse length of 1000 cycles and a repetition rate of 100 Hz for a total duration of 5 s). Three control samples were included as well (Table 2). (i) The 'untreated' sample represents cells which were neither exposed to nanospheres nor to ultrasound; (ii) In the '4 °C' sample cells were incubated with the nanospheres on ice to inhibit constitutive uptake routes such as endocytosis [27]. In addition, these cells were not exposed to ultrasound. Therefore, any fluorescence detected in this sample is due to nanospheres adsorbed extracellularly to the cell membrane. Hence, this sample was included to evaluate whether trypan blue is able to quench the extracellular fluorescence of the nanoparticles. Since quenching requires close contact between the fluorophore and the quencher [28], and since trypan blue cannot cross intact cell membranes, it can be used to discriminate between internalized and extracellularly attached particles [29]. (iii) A third control sample, the 'endocytosis' sample, quantifies nanosphere uptake at 37 °C, allowing constitutive routes to be active, without application of ultrasound. Fig. 4 presents typical examples of histograms of nanoparticle uptake, as obtained by flow cytometry, while Fig. 5 summarizes the results of three experiments.

Table 2
Overview of the samples used in the flow cytometry experiments.

Sample	Nanoparticles	Microbubbles	Ultrasound
Untreated	−	−	−
4 °C	+	−	−
Endocytosis	+	−	−
Unloaded microbubbles + nanoparticles	+	+	+
Nanoparticle-loaded microbubbles	+	+	+

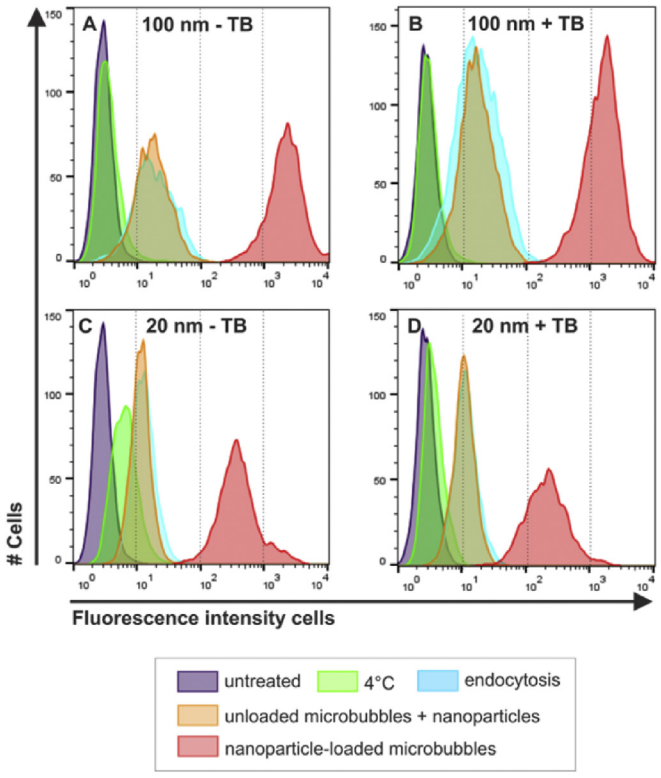

Fig. 4. Representative flow cytometry histograms of the cellular uptake of nanospheres. Uptake of 100 nm nanospheres (A,B) and 20 nm nanospheres (C,D), without (A,C) and with (B,D) trypan blue (TB) quenching of extracellular fluorescence. Uptake of nanospheres was evaluated after mixing the nanospheres with unloaded microbubbles and ultrasound exposure (orange curve) and after loading the nanospheres onto microbubbles followed by ultrasound exposure (red curve). Untreated cells (purple curve), cells incubated with the nanospheres at 4 °C without ultrasound exposure (green curve), and cells incubated with the particles at 37 °C without ultrasound exposure (blue curve) served as control samples. The '4 °C' sample was used to verify whether or not trypan blue quenched extracellular nanoparticle fluorescence. (For interpretation of the references to color in this figure legend, the reader is referred to the web version of this article.)

First of all, the delivery of 100 nm polystyrene nanospheres was studied. Fig. 4A illustrates that the histograms of the 'endocytosis' sample (blue curve) and the 'unloaded microbubbles + nanoparticles' (orange curve) overlap. The cells show a substantially higher fluorescence intensity, thus a larger uptake of nanospheres, when nanospheres were loaded onto microbubbles (red curve). When performing trypan blue quenching (Fig. 4B), the fluorescence intensity of all samples only slightly decreases. It must be noted that the nanospheres showed little extracellular attachment to the cell membrane ('4 °C' sample in Fig. 4A). Hence, this sample was less suited to verify trypan blue quenching. Therefore, we evaluated the quenching potential of trypan blue by measuring the fluorescence intensity of a suspension of nanospheres in the absence and presence of trypan blue (Supplementary Fig. 1). Upon adding trypan blue to the polystyrene spheres, their fluorescence became only partially quenched, which is probably due to the fact that trypan blue cannot penetrate into the solid spheres.

The cellular uptake profiles of 20 nm nanospheres (Fig. 4C and D) were similar to those of 100 nm nanospheres. The 'endocytosis' sample (blue curve) and the 'unloaded microbubbles + nanoparticles' sample (orange curve) again overlapped, while loading the nanoparticles onto the microbubbles (red curve) drastically improved the delivery efficiency. Note that the fluorescence of the cells exposed to microbubbles loaded with the 20 nm nanospheres (red curves in panel C and D of Fig. 4) is lower than the fluorescence of cells exposed to microbubbles loaded with 100 nm nanospheres (red curves in panel A and B of Fig. 4). However, it cannot be concluded that 20 nm nanospheres show less cellular uptake, since one 20 nm nanosphere contains 40 times less fluorescent labels than one 100 nm nanosphere, as stated by the manufacturer. Fig. 5 displays the mean fluorescence intensity (MFI) of the cells and confirms that the uptake of nanospheres was significantly higher upon attaching them to the microbubbles. Cell viability was assessed for all samples in Figs. 4 and 5, using Calcein AM Red™ viability staining. While more cell debris was detected in the ultrasound exposed samples, all gated cells were found to be viable (data not shown).

3.3. Cellular uptake of mRNA-lipoplexes with unloaded or loaded microbubbles

To study the delivery of the mRNA-lipoplexes by flow cytometry, fluorescent lipids were added to the lipoplex formulation, as described in the materials and methods section. However, we could not label the mRNA-lipoplexes as fluorescent as the commercially purchased nanospheres, since this would change the composition of the lipoplexes. Consequently, the cellular fluorescence intensities

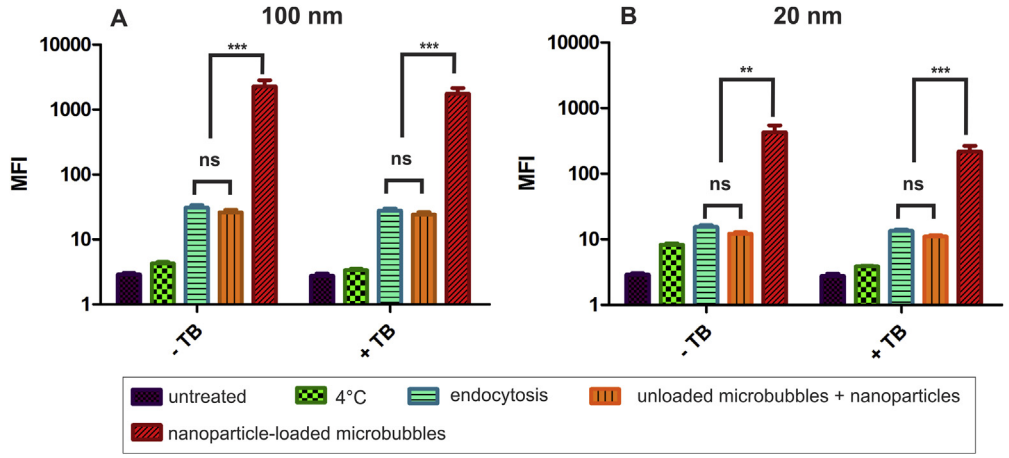

Fig. 5. Mean fluorescence intensity (MFI) of the cells after uptake of the polystyrene nanospheres. Histogram results, as presented in Fig. 4, obtained in three independent experiments were averaged and presented as MFI ± SD. Statistical analysis was performed via a One-way ANOVA tests with a Bonferroni multiple comparison test. *ns* not significant, $^{**}p < 0.01$, $^{***}p < 0.001$.

due to uptake of mRNA-lipoplexes cannot be directly compared to those due to nanopshere uptake.

Fig. 6A illustrates that the histogram of the 'endocytosis' sample (blue curve) overlaps with that of the 'unloaded microbubbles + nanoparticles' sample (orange curve). As for the polystyrene nanospheres, loading the lipoplexes onto the microbubbles (red curve) enhanced the delivery markedly. When trypan blue was added (Fig. 6B), the '4 °C' histogram shifted to lower fluorescence intensities. This indicates that quenching of the extracellularly attached lipoplexes was successful, as confirmed in a separate quenching experiment (Supplementary Fig. 1). Remarkably, the fluorescence of cells exposed to microbubbles loaded with mRNA-lipoplexes became significantly quenched by trypan blue, even to such an extent that the histogram overlapped with the histograms of the 'endocytosis' sample and the 'unloaded microbubbles + nanoparticles' sample (Fig. 6B). Fig. 7B confirms that there was no longer a statistical difference between the MFI-values. These observations suggest that, when using mRNA-lipoplex-loaded microbubbles, the mRNA-lipoplexes are initially associated with the cell membrane upon applying ultrasound, rather than being intracellularly delivered.

Because mRNA should enter the cellular cytoplasm to be translated into proteins, we evaluated whether the cell membrane bound lipoplexes were trafficked intracellularly as a function of time. For this, the samples were analyzed 8 h, 16 h and 24 h after ultrasound exposure. Generally, the fluorescence intensity of most samples decreased with time (compare Fig. 6A versus 6C,E,G; and compare Fig. 6B versus 6D,F,H). This may be caused by cell division, thereby decreasing the mean fluorescence intensity per cell. More interestingly, starting from 8 h after ultrasound exposure and in the presence of trypan blue, the histogram of the 'loaded microbubbles' sample did no longer overlap with histograms of the 'endocytosis' and 'unloaded microbubbles + nanoparticles' sample (compare Fig. 6B versus Fig. 6D,F,H). This demonstrates that with the loaded microbubbles an increased amount of internalized lipoplexes was observed, since this sample showed less quenching. The MFI increase compared to the 'endocytosis' and 'unloaded microbubbles + nanoparticles' sample was twofold at 8 h and threefold after 16 h or 24 h (Fig. 7B). Therefore, our results suggest that, when using mRNA-lipoplex-loaded microbubbles, the mRNA-lipoplexes are initially associated with the cell membrane upon applying ultrasound (as explained above, based on Fig. 6B) and become subsequently internalized in the following hours.

3.4. *Real-time confocal imaging of cells exposed to ultrasound and polystyrene nanospheres*

Using real-time swept field confocal microscopy during ultrasound radiation, we aimed to investigate more in depth the microbubble-cell interactions and the drug delivery mechanisms taking place when the polystyrene nanospheres are either mixed with or loaded onto microbubbles. For this, green fluorescent nanospheres were used, while the microbubble shell and the cell membrane were both labeled in red.

Fig. 8 shows a typical result of unloaded microbubbles mixed with polystyrene nanopsheres. In this example, two large microbubble clusters are present at both sides of the cell (middle row, frame 1). When the microbubbles start to oscillate, they release a part of their shell material (middle row, frame 2, dotted arows). More importantly, the nanospheres in the cell surroundings start to move very rapidly (bottom row – see also real-time recordings provided in Supplementary Video 1). In frame 3 and 4, bottom row, the nanospheres (arrows) arrive at the cell (delineated by the yellow line (in web version)). Subsequently, they are transported away again. As soon as ultrasound is turned off, the rapid flow stops. This

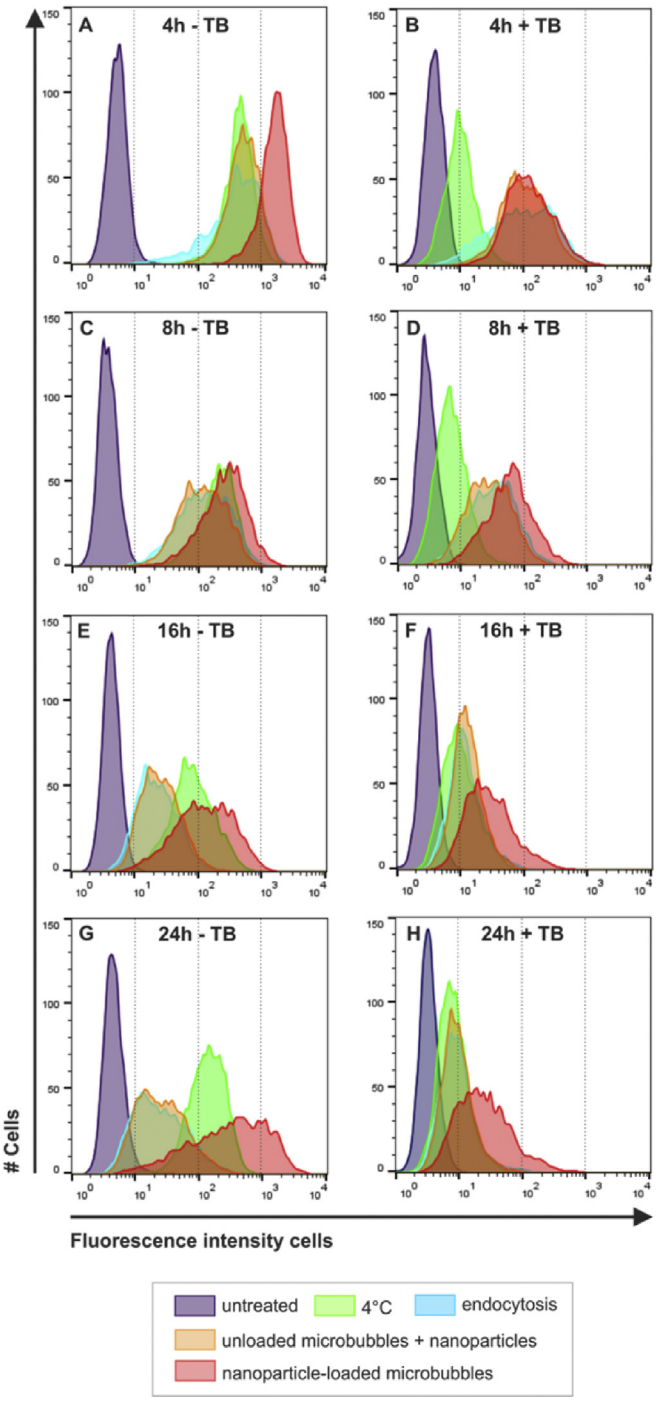

Fig. 6. Representative flow cytometry histograms of the cellular uptake of mRNA-lipoplexes. Uptake of mRNA-lipoplexes was assessed without (left column) or with (right column) trypan blue (TB) quenching of extracellular fluorescence. Samples were analyzed at 4 h (A,B), 8 h (C,D), 16 h (E,F) and 24 h (G,H) after ultrasound exposure. Uptake of mRNA-lipoplexes was evaluated after mixing the lipoplexes with unloaded microbubbles and ultrasound exposure (orange curve) and after loading the lipoplexes onto microbubbles followed by ultrasound exposure (red curve). Untreated cells (purple curve), cells incubated with mRNA-lipoplexes at 4 °C without ultrasound exposure (green curve) and cells incubated with the lipoplexes at 37 °C without ultrasound exposure (blue curve) served as control samples. The '4 °C' sample was used to verify whether or not trypan blue quenched extracellular fluorescence. (For interpretation of the references to color in this figure legend, the reader is referred to the web version of this article.)

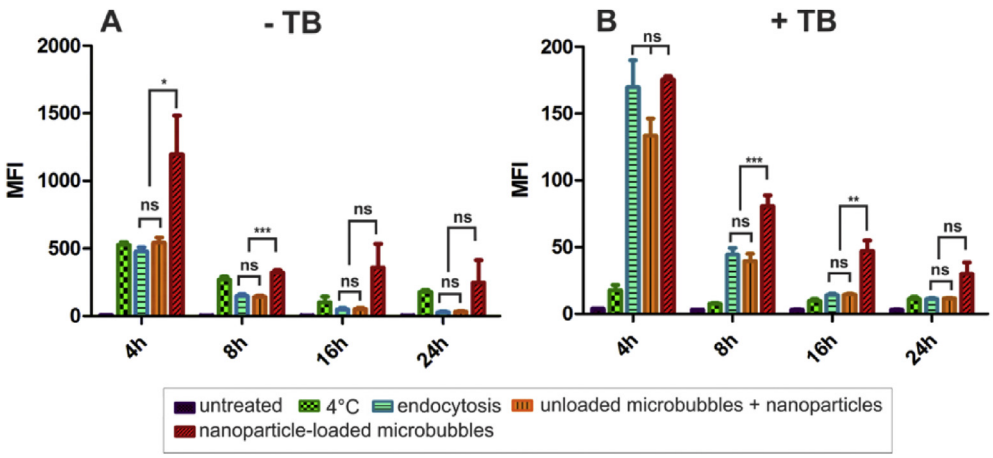

Fig. 7. Mean fluorescence intensity (MFI) of the cells after uptake of the mRNA-lipoplexes. Histogram results, as presented in Fig. 6, obtained in three independent experiments were averaged and presented as mean fluorescence intensity (MFI) ± SD. Statistical analysis was performed via a One-way ANOVA tests with a Bonferroni multiple comparison test. *ns* not significant, $^{*}p < 0.05$, $^{**}p < 0.01$, $^{***}p < 0.001$. Note that the scale of the two graphs is different. Due to trypan blue quenching, the samples in graph (B) show less fluorescence.

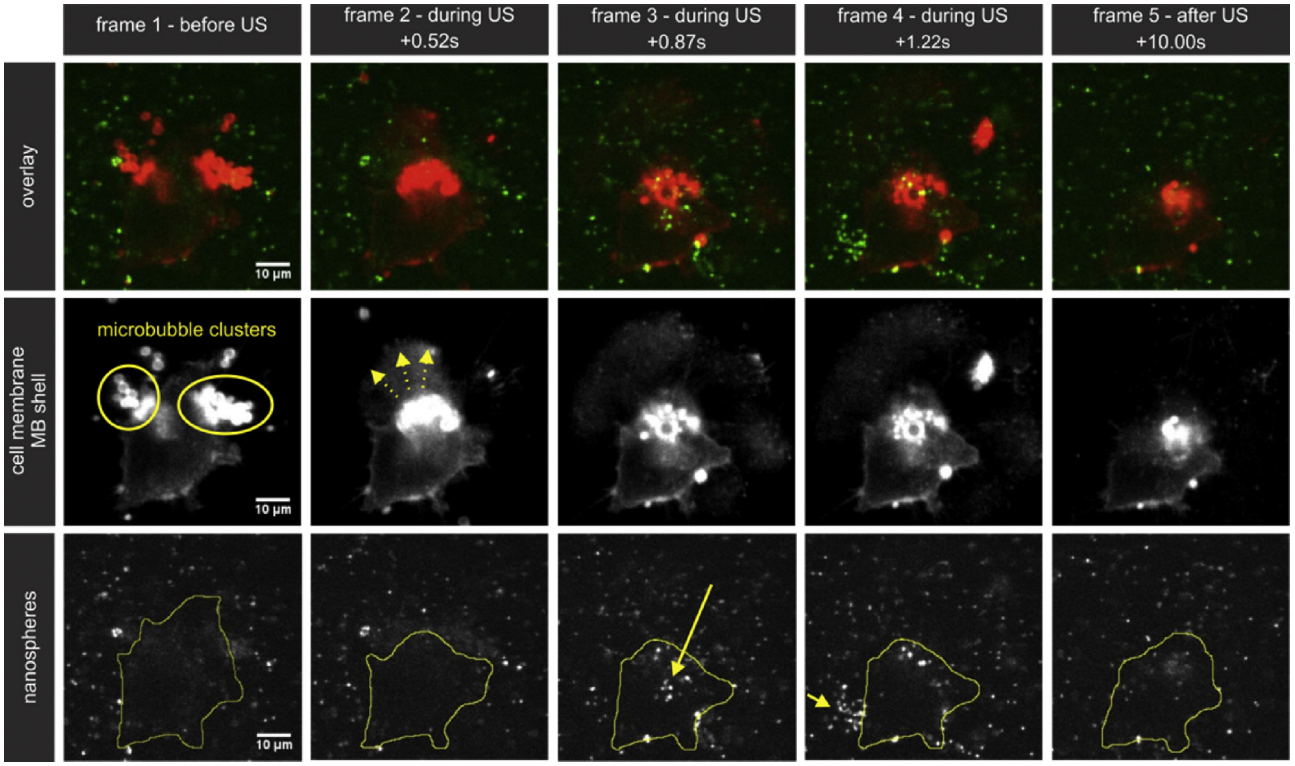

Fig. 8. Unloaded microbubbles + nanospheres. Time-lapse series showing rapid movement of nanospheres (indicated with arrows) upon microbubble cavitation. (top row) The overlay of red and green fluorescent confocal images, (middle row) the red fluorescent cell membrane and microbubble shell, (bottom row) the green fluorescent nanospheres. The cell contour is delineated with a line in the bottom row images. To perceive the motion of the nanospheres more clearly, the reader is referred to the real-time recording provided in Supplementary Video 1, which is a representative example of the microbubble-cell interactions observed when microbubbles and nanospheres are co-administered.

flow is probably caused by the microstreamings generated by microbubble cavitation, which transport the nanoparticles along with them. Although the microbubbles clearly affected the cell, we could not observe an explicit delivery of nanospheres to the cells, since most nanospheres kept on showing Brownian motion after turning off ultrasound. If the particles would be delivered in the cell, their movement would be restricted due to e.g. binding to intracellular components and steric hindrance.

Supplementary data related to this article can be found online at http://dx.doi.org/10.1016/j.biomaterials.2016.01.022.

In addition, real-time swept field confocal microscopy experiments were performed on microbubbles loaded with polystyrene nanospheres, in which two phenomena were observed. First, upon applying ultrasound, release of green fluorescent nanospheres from red fluorescent microbubbles was observed, which is illustrated by a representative example in Fig. 9 and Supplementary Video 2. Both microbubbles in Fig. 9 have nanospheres attached to their shell, since the red fluorescence of the microbubble shell co-localizes with the green fluorescence of the nanospheres. Upon ultrasound exposure, the largest microbubble (bottom row, arrow) locally

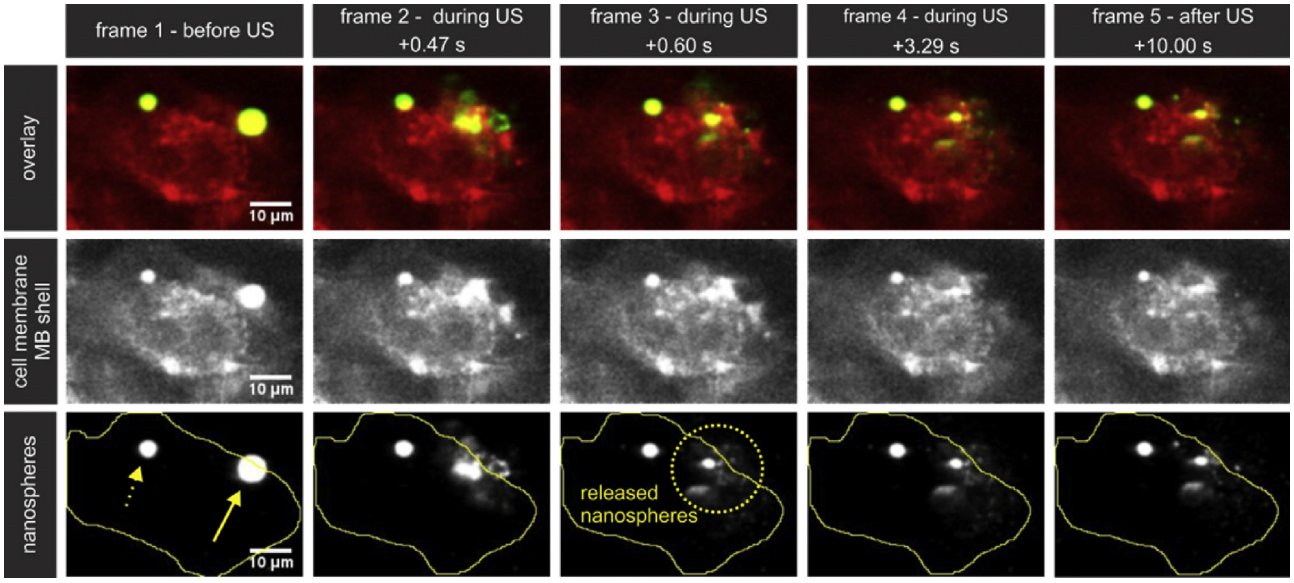

Fig. 9. Release of nanospheres from loaded microbubbles. Selected frames from a real-time confocal recording displaying the local release of nanospheres from a loaded microbubble. After release from the microbubble, the nanospheres do not become associated with the cell, since they keep on showing Brownian diffusion. The selected frames are confocal images of (top row) the overlay of red and green fluorescence, (middle row) the red fluorescent cell membrane and microbubble shell, (bottom row) the green fluorescent nanospheres. The cell contour, as defined by the red cell membrane staining, is delineated with a line in the bottom row images. To perceive the motion of the nanospheres more clearly, the reader is referred to the real-time recording provided in Supplementary Video 2, which is a representative example of the microbubble-cell interactions observed with the loaded microbubbles.

releases a cloud of nanospheres (bottom row, dotted circle). It is unclear from the images if the microbubble implodes or if it shrinks to a finite bubble size. The cloud spreads and the nanospheres start to experience Brownian motion in the cell surroundings. Hence, the particles do not seem to become associated with the cell and cellular delivery was not detected. The smaller microbubble (bottom row, dotted arrow) did not release their nanospheres. This might be due to a mismatch between its resonance frequency and the driving ultrasound frequency. It was reported that microbubbles only release shell materials if their oscillation amplitude is above a certain threshold [22]. In addition, it is well-known from literature that the oscillation amplitude is largest when the ultrasound driving frequency matches the resonance frequency of the microbubbles, which depends on their size [1].

Supplementary data related to this article can be found online at http://dx.doi.org/10.1016/j.biomaterials.2016.01.022.

Besides release of the nanospheres, a second interesting phenomenon was observed when using nanosphere-loaded microbubbles, as presented in Supplementary Video 3 and depicted in Fig. 10. Upon ultrasound exposure, the microbubble indicated with the arrow (bottom row) translates towards the cell, while depositing its cargo directly onto the cell. The elongated patch of green fluorescent nanospheres (bottom row, dotted circle) is attached to the cell, since the nanospheres are no longer moving. In similarity to the work of Hu et al. [30], we see the formation of a cell membrane pore, visible as a black hole in the red-labeled cell membrane (middle row, dotted arrow). The nanospheres are, however, not co-localized with the cell membrane disruption. This suggests that passive diffusion through cell membrane damages is not the main mechanism causing nanoparticle delivery. The smaller microbubbles, below resonant size, are again not driven by the applied ultrasound.

Supplementary data related to this article can be found online at http://dx.doi.org/10.1016/j.biomaterials.2016.01.022.

3.5. Real-time confocal imaging of cells exposed to ultrasound and mRNA-lipoplexes

Since the mRNA-lipoplexes could not be sufficiently labeled to be imaged individually, recordings of cells to which mRNA-lipoplexes and unloaded microbubbles were added were not informative. However, packing the lipoplexes onto the microbubble shell resulted in a sufficiently high green fluorescence to enable real-time confocal imaging of cells exposed to mRNA-lipoplex-loaded microbubbles. In essence, similar phenomena as for the nanosphere-loaded microbubbles were observed: upon applying ultrasound, release of the mRNA-lipoplexes from the microbubble shell, as well as direct deposition of the nanoparticles onto the cells was observed. A representative example of both events is provided in Supplementary Videos 4 and 5, respectively, and the corresponding Figs. 11 and 12. In Fig. 11, before ultrasound exposure, the cell already shows some green fluorescent staining, probably due to the endocytic uptake of free lipoplexes which were not attached to microbubbles (bottom row, frame 1), resulting in the appearance of fluorescent intracellular vesicles. In frame 2, the two lipoplex-loaded microbubbles (bottom row, dotted circle) implode, thereby locally releasing lipoplex aggregates. In the following frames of the bottom row, some of these aggregates move away from the cell (full arrow) and eventually out of the field of view (frame 6), while one aggregate stays localized at the cell border (dotted arrow). The image series depicted in Fig. 12 illustrates direct deposition of the lipoplexes. Upon ultrasound exposure, the loaded microbubble indicated with the full arrow projects the lipoplexes in a patch onto the cell (bottom row, dotted circle). The other microbubble (bottom row, dotted arrow) also seems to deliver the lipoplexes to the cell, although this event is slightly out of focus.

Supplementary data related to this article can be found online at http://dx.doi.org/10.1016/j.biomaterials.2016.01.022.

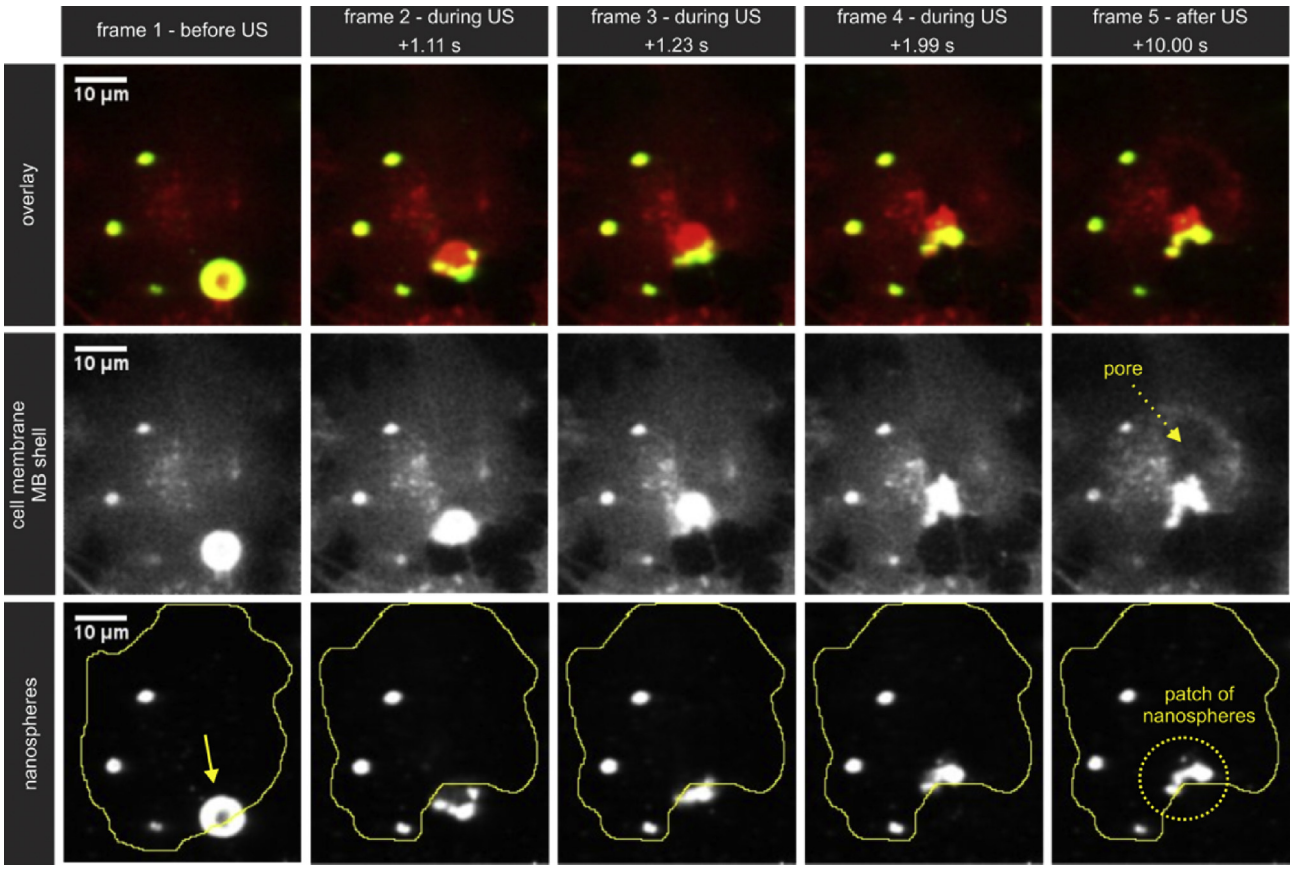

Fig. 10. Direct deposition of nanospheres onto cells by loaded microbubbles. These series of confocal images display an example of the deposition of a patch of nanospheres onto the cell upon ultrasound exposure. The nanospheres are not co-localized with the created pore in the cell membrane, detected in the red fluorescent channel (dotted arrow). The confocal images are (top row) the overlay of red and green fluorescence, (middle row) the red fluorescent cell membrane and microbubble shell, (bottom row) the green fluorescent nanospheres. The cell contour, as defined by the red cell membrane staining, is delineated with a line in the bottom row images. To perceive these observations more clearly, the reader is referred to the real-time recording provided in Supplementary Video 3, which is a representative example of the microbubble-cell interactions observed with the loaded microbubbles.

4. Discussion

4.1. Unloaded microbubbles and nanoparticles

In most studies on ultrasound mediated drug delivery, drugs are simply mixed with the microbubbles. Although this approach has definitely been proven to be successful [31], our observations show that mixing polystyrene nanospheres and mRNA-lipoplexes (Figs. 5 and 7, respectively) with unloaded microbubbles does not improve the delivery of these nanomaterials to cells. This is in line with other studies which demonstrated that unloaded microbubbles are less effective in enhancing the cellular delivery of larger molecules [3,14]. Recently, we found that two cellular routes are involved in the uptake of relatively small FITC-dextrans when they are mixed with unloaded microbubbles followed by ultrasound application [5]: passive diffusion through membranes pores and enhanced endocytosis. As the membrane pores act as a sieve, it is more difficult for larger molecules or nanoparticles to access them, which might explain why the mixing of nanospheres or mRNA-lipoplexes with unloaded microbubbles does not improve their intracellular delivery.

4.2. Nanoparticle-loaded microbubbles

When using nanosphere- or mRNA-lipoplex-loaded microbubbles, delivery to the cells substantially improved, as summarized in Figs. 5 and 7, respectively. Real-time recordings during ultrasound exposure revealed that this may be caused by two phenomena: (i) local release of the nanospheres and mRNA-lipoplexes from the microbubbles in the cell surroundings (Fig. 9 and Supplementary Video 2, Fig. 11 and Supplementary Video 4, respectively); and (ii) 'direct' deposition of the nanospheres and mRNA-lipoplexes onto the cell (Fig. 10 and Supplementary Video 3, Fig. 12 and Supplementary Video 5, respectively). Release from loaded microbubbles has been reported before [22–24], as also mentioned in the introduction. It locally increases the free drug concentration, which may aid in drug delivery. However, cellular uptake via membrane pores or endocytosis is still required and may encounter the same hurdles as when the drug is mixed with unloaded microbubbles. In contrast, in the 'direct' deposition phenomenon a substantial number of nanoparticles were deposited directly on the cell upon applying ultrasound to loaded microbubbles. To the best of our knowledge, this phenomenon has not been described before. We suggest to call this 'sonoprinting', as fluorescent particles are projected in patches onto the cell. In a study by Lum et al. [32], the authors demonstrated that microbubbles having nanobeads attached to their shell were able to deposit a large amount of the nanobeads onto the surface of a cellulose tube. Moreover, the deposition of beads co-localized with fluorescent components of the microbubble shell, indicating that lipid shell fragments were expelled together with the attached particles. Furthermore, Ibsen et al. [33] observed elongated

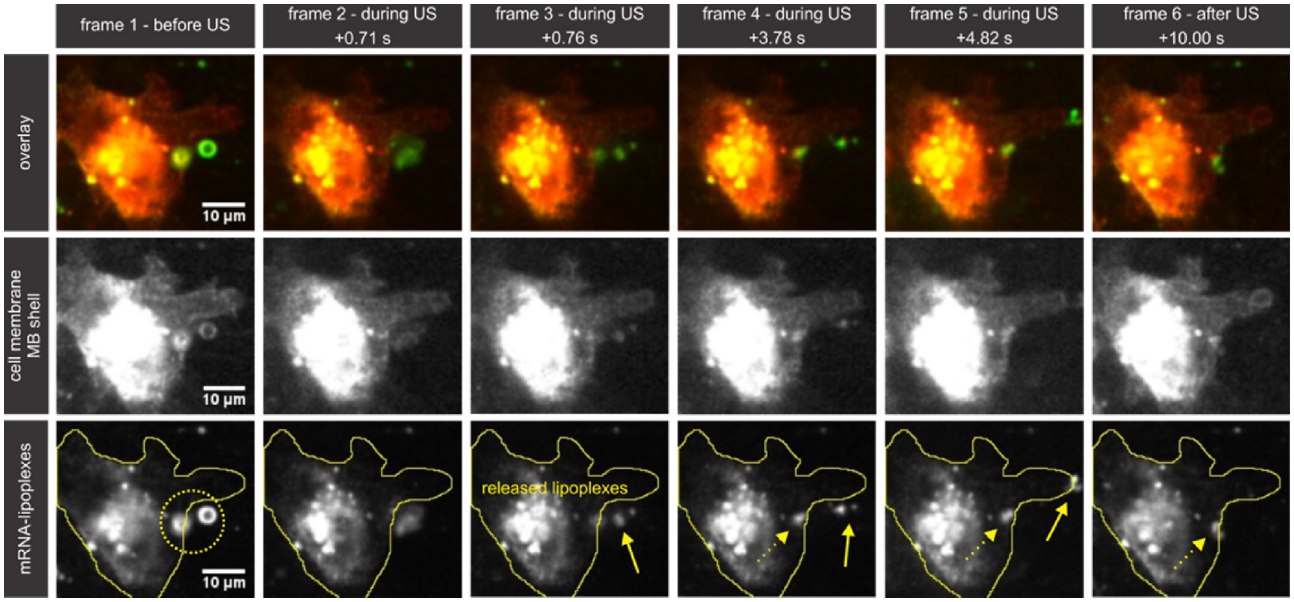

Fig. 11. Release of mRNA-lipoplexes from loaded microbubbles. Upon ultrasound exposure, the two microbubbles locally release mRNA-lipoplexes, similarly to the release of nanospheres. The lipoplexes indicated with the arrow are not associated with the cell since they are moving out of the field of view over time. One lipoplex aggregate (dotted arrow) remains at the cell border. The confocal images are (top row) the overlay of red and green fluorescence, (middle row) the red fluorescent cell membrane and microbubble shell, (bottom row) the green fluorescent nanospheres. The cell contour, as defined by the red cell membrane staining, is delineated with a line in the bottom row images. To perceive these observations more clearly, the reader is referred to the real-time recording provided in Supplementary Video 4, which is a representative example of the microbubble-cell interactions observed with the loaded microbubbles.

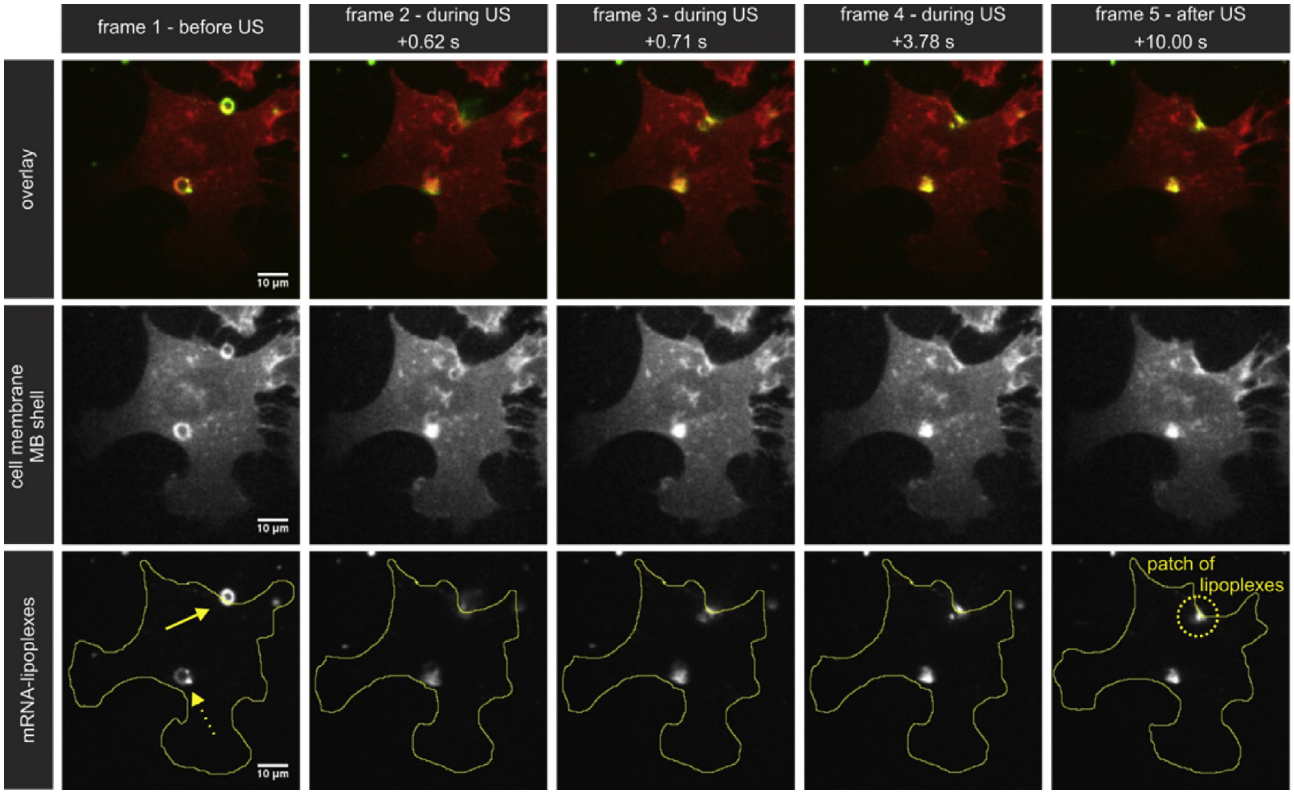

Fig. 12. Direct deposition of mRNA-lipoplexes onto cells by loaded microbubbles. This image sequence displays the direct deposition of a patch of lipoplexes onto the cell by the loaded microbubble indicated with the full arrow. The confocal images are (top row) the overlay of red and green fluorescence, (middle row) the red fluorescent cell membrane and microbubble shell, (bottom row) the green fluorescent nanospheres. The cell contour, as defined by the red cell membrane staining, is delineated with a line in the bottom row images. To perceive these observations more clearly, the reader is referred to the real-time recording provided in Supplementary Video 5.

fluorescent patches on cells after exposing them to fluorescently labeled lipid microbubbles and ultrasound, comparable to the patches of polystyrene nanospheres and mRNA-lipoplexes observed in Figs. 10 and 12, respectively. Moreover, using nanoemulsion droplets carrying fluorescein and vaporized by ultrasound, Couture et al. similarly observed fluorescein deposited onto the membrane surface of an Opticell; and even into tissue after intravenous injection of the droplets in a chicken embryo [34]. The 'sonoprinting' phenomenon is also in agreement with previous results from our group with pDNA-lipoplex-loaded microbubbles, where the pDNA-lipoplexes seemed to be embedded in the cell membrane immediately after ultrasound exposure [35]. Importantly, the pDNA-lipoplexes must have been trafficked intracellularly afterward, since a substantial protein expression was observed. The results described in this study and the above-mentioned examples suggest that 'sonoprinting' might be an important mechanism in the delivery process of the nanoparticles using nanoparticle-loaded microbubbles.

Apart from the real-time confocal imaging performed in this study, fluorescence real-time imaging at much faster frame rates will be required to fully capture which microbubble behavior is exactly responsible for the observed phenomena. Several biophysical microbubble-cell interactions haven been suggested to contribute to ultrasound assisted drug delivery, as mentioned in the introduction, including microstreaming around cavitating microbubbles, microbubble jetting and microbubble translation driven by acoustic radiation forces [1]. Microstreaming creates fluid motion in the microbubble surroundings, which may transport released drugs from loaded microbubbles [22]. The presence and the patterns of microstreaming have been studied before; and flow velocities of 8–80 mm/s were reported [22,36,37]. In this study, the fast motion of the nanoparticles observed in Fig. 8 and Supplementary Video 1 could also be attributed to microstreaming. However, in the 'sonoprinting' phenomenon, the elongated patches are projected in one single direction, implicating that microstreamings are probably not involved in the transport. Schutt et al. [38] suggested that jetting accounted for the elongated microbubble debris clouds they observed after ultrasound exposure. Jetting occurs at higher acoustic pressures when a microbubble collapses asymmetrically near a boundary. It consists of the projection of a liquid jet towards the boundary [2]. Furthermore, it is well known from literature that ultrasound exposure exerts a radiation force upon microbubbles [1], which can induce microbubble displacement over several micrometer when exposed to successive ultrasound cycles [39]. As we used relatively long ultrasound pulses (1000 cycles) in this study, it is very likely that microbubble translation occurred, which may also contribute to the observed effects.

We propose 'sonoprinting' as a mechanism with different features from the generally accepted mechanisms of drug delivery by ultrasound and microbubbles, i.e. the formation of cell membrane pores ('sonoporation') and enhanced endocytosis. The real-time imaging data (Figs. 10 and 12) showed that the nanoparticles were directly transferred from the loaded microbubbles onto the cells in patches. This cellular delivery pattern is different from the cellular uptake pattern when molecules are mixed with unloaded microbubbles and delivered by sonoporation or endocytosis [4]. In a previous study [5], we observed with confocal microscopy that the uptake of FITC-dextrans via sonoporation resulted in fluorescence spread throughout the cell due to passive diffusion through the cell membrane pores. Furthermore, the endocytic uptake of FITC-dextrans resulted in the appearance of fluorescent intracellular vesicles. In contrast, via sonoprinting the nanoparticles were delivered in patches to the cell membrane. Moreover, the quenching experiments (Figs. 6 and 7) suggest that the nanoparticles were initially associated with the membrane of the cell, and not delivered intracellularly. The nanoparticles only became internalized in the following hours. If the uptake would occur via passive diffusion through cell membrane pores, the intracellular concentration would be expected to reach high levels immediately after ultrasound exposure, since diffusion is a fast process and pore closure is reported to occur within seconds to minutes [3,30].

How intracellular trafficking took place following deposition of the nanoparticles onto the cell membrane was not assessed in the present study. It could be that endocytosis is playing a role. However, by using an endocytosis inhibitor, previous research in our group with pDNA-lipoplex-loaded microbubbles indicated that endocytosis was not involved in the transfection of these pDNA-lipoplexes [35]. In another study we loaded AAV-viruses onto lipid microbubbles [40]. For AAV it is known that the viruses should be endocytosed to transduct the cells. Applying ultrasound to the AAV-loaded microbubbles did not transduct melanoma cells, while the cells clearly showed AAV uptake. These results indicated that they were delivered to the cells by a mechanism different from endocytosis. Recently, it has been proposed that lipid nanoparticles can deliver their content by membrane fusion [41–43]. Via this pathway, the lipids of the nanoparticle are exchanged or mixed with the lipids of the cell membrane, leading to cytosolic delivery and avoiding endocytic uptake and endosomal degradation. We hypothesize that lipid-fusion might contribute to the intracellular trafficking of the lipoplexes after 'sonoprinting'.

As we used both unloaded and loaded microbubbles in this study, one could wonder whether or not a different acoustic response could have influenced the observed effects. First, microbubble loading may change microbubble size and thus resonance frequency, i.e. the frequency at which the microbubbles show their highest response [1]. However, the mean size before and after microbubble loading did not differ notably. Moreover, the polydispersity of the formulations ensures that there is always a certain fraction of microbubble population responding to the applied ultrasound. Second, loaded microbubbles were reported to have a higher pressure threshold for the onset of microbubble oscillation [44]. However, in this study an acoustic pressure of 300 kPa was used, which is substantially higher than the reported threshold of 50–70 kPa. However, small differences in amplitude of oscillation between the unloaded and the loaded microbubbles cannot be excluded.

In this study, cells were cultured on a rigid membrane, which is typically the case for *in vitro* experiments, while *in vivo* the encountered boundaries are usually softer. Although it is reported that biophysical effects, such as microbubble translation [45,46] and microjetting [47] also occur *in vivo*, it is expected that they are influenced by the elasticity of the boundary. For example, it was observed that the liquid jet in microjetting is pointing towards a rigid boundary [48], while in excised tissue it was pointing away from the softer vessel wall [47]. These issues highlight the need for the use of more complex *in vivo*-like cell culture models in future research in this field. Nevertheless, there may be some targets *in vivo* where more rigid boundaries could be encountered which resemble more the *in vitro* conditions, for example near blood clots or atherosclerotic plaques. A second aspect which needs to be brought into account when extrapolating our findings to *in vivo* conditions, is the blood flow, as microbubbles are typically injected intravenously. When unloaded microbubbles are mixed with drugs and co-injected, the drugs are diluted in the blood, while drug-loaded microbubbles have the advantage that the drug concentration near the microbubble is very high due to local drug release upon ultrasound exposure. Therefore, the drugs can benefit more from the biophysical effects created by microbubble cavitation compared to drugs co-administered with microbubbles. Moreover,

these biophysical effects, such as microstreaming [22], microjetting [1] and microbubble translation [39] are still relevant *in vivo* as their associated velocities are generally higher than the blood flow velocity. In addition, blood flow can hinder the close contact between cells and microbubbles. As in most sonoprinting cases the microbubbles were in the vicinity of the cells, this close contact seems to promote the nanoparticle delivery, which can be ensured *in vivo* by using targeted microbubbles. A third aspect in the extrapolation to *in vivo* applications is the fact that the microbubbles were adjacent to the cell monolayer in our *in vitro* experiments. As microbubbles are confined to the blood pool when injected intravenously, an *in vivo* target could be cells of the endothelium, which forms the inner lining of the blood vessels and which is an interesting target in cardiovascular diseases. For example, researchers are exploring ultrasound and microbubble mediated gene delivery to endothelial cells in cardiac tissue to induce angiogenesis and stimulate reperfusion after myocardial infarct [49,50]. Another interesting type of target cells to which microbubbles can have direct access are immune cells. Our research group recently showed that subcutaneously injected microbubbles drain to the lymphatic vessels, which harbor large numbers of dendritic cells, the key players in initiating immune responses [20]. Moreover, we have shown that by using mRNA-lipoplex-loaded microbubbles, similar to those used in this study, dendritic cells can be successfully transfected in order to initiate anti-tumor immune responses [51].

5. Conclusion

It has been proven that mixing drugs with microbubbles followed by ultrasound exposure can enhance drug delivery [1,31]. However, this 'co-administration mode' may only be useful when using small drug molecules, as these can easily diffuse through the membrane pores created by the cavitating microbubbles. Our findings demonstrate that ultrasound improves the cellular delivery of larger nanoparticles, like polystyrene spheres and mRNA-lipoplexes, only when these were loaded onto microbubbles. Real-time imaging during ultrasound exposure revealed that 'sonoprinting' might be an important mechanism in the delivery process with nanoparticle-loaded microbubbles. We have defined 'sonoprinting' as the direct deposition of patches of nanoparticles onto the cell upon applying ultrasound to the nanoparticle-loaded microbubbles. After this initial deposition, the nanoparticles become internalized in the cells.

Acknowledgments

Ine De Cock is a doctoral fellow of the Institute for the Promotion of Innovation through Science and Technology in Flanders, Belgium (IWT-Vlaanderen). Ine Lentacker is a postdoctoral fellow of the Research Foundation Flanders, Belgium (FWO-Vlaanderen). The support of both these institutions is gratefully acknowledged. This work is also supported by NanoNextNL, a micro and nanotechnology consortium of the Government of the Netherlands and 130 partners.

Appendix A. Supplementary data

Supplementary data related to this article can be found at http://dx.doi.org/10.1016/j.biomaterials.2016.01.022.

References

[1] K. Kooiman, H.J. Vos, M. Versluis, N. de Jong, Acoustic behavior of microbubbles and implications for drug delivery, Adv. Drug Deliv. Rev. 72 (2014) 28–48.
[2] I. Lentacker, I. De Cock, R. Deckers, S.C. De Smedt, C.T.W. Moonen, Understanding ultrasound induced sonoporation: definitions and underlying mechanisms, Adv. Drug Deliv. Rev. 72 (2014) 49–64.
[3] S. Mehier-Humbert, T. Bettinger, F. Yan, R.H. Guy, Plasma membrane poration induced by ultrasound exposure: implication for drug delivery, J. Control. Release 104 (1) (2005) 213–222.
[4] B.D. Meijering, L.J. Juffermans, A. van Wamel, R.H. Henning, I.S. Zuhorn, M. Emmer, A.M. Versteilen, W.J. Paulus, W.H. van Gilst, K. Kooiman, N. de Jong, R.J. Muster, L.E. Deelman, O. Kamp, Ultrasound and microbubble-targeted delivery of macromolecules is regulated by induction of endocytosis and pore formation, Circ. Res. 104 (5) (2009) 679–687.
[5] I. De Cock, E. Zagato, K. Braeckmans, Y. Luan, N. de Jong, S.C. De Smedt, I. Lentacker, Ultrasound and microbubble mediated drug delivery: acoustic pressure as determinant for uptake via membrane pores or endocytosis, J. Control. Release 197 (2015) 20–28.
[6] A. van Wamel, K. Kooiman, M. Harteveld, M. Emmer, F.J. ten Cate, M. Versluis, N. de Jong, Vibrating microbubbles poking individual cells: drug transfer into cells via sonoporation, J. Control. Release 112 (2) (2006) 149–155.
[7] R.K. Schlicher, H. Radhakrishna, T.P. Tolentino, R.P. Apkarian, V. Zarnitsyn, M.R. Prausnitz, Mechanism of intracellular delivery by acoustic cavitation, Ultrasound Med. Biol. 32 (6) (2006) 915–924.
[8] I. Lentacker, S.C. De Smedt, N.N. Sanders, Drug loaded microbubble design for ultrasound triggered delivery, Soft Matter. 5 (2009) 2161–2170.
[9] E.C. Unger, T.P. McCreery, R.H. Sweitzer, V.E. Caldwell, Y. Wu, Acoustically active lipospheres containing paclitaxel: a new therapeutic ultrasound contrast agent, Invest. Radiol. 33 (12) (1998) 886–892.
[10] Y.Z. Zhao, H.D. Liang, X.G. Mei, M. Halliwell, Preparation, characterization and in vivo observation of phospholipid-based gas-filled microbubbles containing hirudin, Ultrasound Med. Biol. 31 (9) (2005) 1237–1243.
[11] J.P. Christiansen, B.A. French, A.L. Klibanov, S. Kaul, J.R. Lindner, Targeted tissue transfection with ultrasound destruction of plasmid-bearing cationic microbubbles, Ultrasound Med. Biol. 29 (12) (2003) 1759–1767.
[12] A. Kheirolomoom, P.A. Dayton, A.F. Lum, E. Little, E.E. Paoli, H. Zheng, K.W. Ferrara, Acoustically-active microbubbles conjugated to liposomes: characterization of a proposed drug delivery vehicle, J. Control. Release 118 (3) (2007) 275–284.
[13] B. Geers, I. Lentacker, S. Cool, J. Demeester, S.C. De Smedt, N.N. Sanders, Ultrasound responsive doxorubicin-loaded microbubbles; towards an easy applicable drug delivery platform, J. Control. Release 148 (1) (2010) 59–60.
[14] I. Lentacker, S.C. De Smedt, J. Demeester, V. Van Marck, M. Bracke, N.N. Sanders, Lipoplex-loaded microbubbles for gene delivery: a trojan horse controlled by ultrasound, Adv. Funct. Mater. 17 (12) (2007) 1910–1916.
[15] I. Lentacker, B. Geers, J. Demeester, S.C. De Smedt, N.N. Sanders, Design and evaluation of doxorubicin-containing microbubbles for ultrasound-triggered doxorubicin delivery: cytotoxicity and mechanisms involved, Mol. Ther. 18 (1) (2010) 101–108.
[16] S.R. Sirsi, M.A. Borden, State-of-the-art materials for ultrasound-triggered drug delivery, Adv. Drug Deliv. Rev. 72 (2014) 3–14.
[17] J.J. Rychak, A.L. Klibanov, Nucleic acid delivery with microbubbles and ultrasound, Adv. Drug Deliv. Rev. 72 (2014) 82–93.
[18] I. Lentacker, B.G. De Geest, R.E. Vandenbroucke, L. Peeters, J. Demeester, S.C. De Smedt, N.N. Sanders, Ultrasound-responsive polymer-coated microbubbles that bind and protect DNA, Langmuir 22 (17) (2006) 7273–7278.
[19] F. Kiessling, S. Fokong, P. Koczera, W. Lederle, T. Lammers, Ultrasound microbubbles for molecular diagnosis, therapy, and theranostics, J. Nucl. Med. 53 (3) (2012) 345–348.
[20] H. Dewitte, K. Vanderperren, H. Haers, E. Stock, L. Duchateau, M. Hesta, J.H. Saunders, S.C. De Smedt, I. Lentacker, Theranostic mRNA-loaded microbubbles in the lymphatics of dogs: implications for drug delivery, Theranostics 5 (1) (2015) 97–109.
[21] J.R. Eisenbrey, M.C. Soulen, M.A. Wheatley, Delivery of encapsulated Doxorubicin by ultrasound-mediated size reduction of drug-loaded polymer contrast agents, IEEE Trans. Biomed. Eng. 57 (1) (2010) 24–28.
[22] Y. Luan, G. Lajoinie, E. Gelderblom, I. Skachkov, A.F. van der Steen, H.J. Vos, M. Versluis, N. De Jong, Lipid shedding from single oscillating microbubbles, Ultrasound Med. Biol. 4 (8) (2014) 1834–1846.
[23] Y. Luan, G. Lajoinie, E. Gelderblom, I. Skachkov, H. Dewitte, I. Lentacker, T. van Rooij, H. Vos, T. van der Steen, M. Versluis, N. de Jong, Liposome shedding from a vibrating microbubble on nanoseconds timescale, in: IEEE Ultrasonics Symposium Proceedings, 2013. Czech Republic (Prague) IUS1-B1-2.
[24] M.A. Borden, D.E. Kruse, C.F. Caskey, S. Zhao, P.A. Dayton, K.W. Ferrara, Influence of lipid shell physicochemical properties on ultrasound-induced microbubble destruction, IEEE Trans. Ultrason. Ferroelectr. Freq. Control 52 (11) (2005) 1992–2002.
[25] M.L. De Temmerman, H. Dewitte, R.E. Vandenbroucke, B. Lucas, C. Libert, J. Demeester, S.C. De Smedt, I. Lentacker, J. Rejman, mRNA-lipoplex loaded microbubble contrast agents for ultrasound-assisted transfection of dendritic cells, Biomaterials 32 (34) (2011) 9128–9135.
[26] P.H. Quax, G.N. van Muijen, E.J. Weening-Verhoeff, L.R. Lund, K. Danø, D.J. Ruiter, J.H. Verheijen, Metastatic behavior of human melanoma cell lines in nude mice correlates with urokinase-type plasminogen activator, its type-1 inhibitor, and urokinase-mediated matrix degradation, J. Cell Biol. 115 (1) (1991) 191–199.
[27] P.H. Weigel, J.A. Oka, Temperature dependence of endocytosis mediated by

the asialoglycoprotein receptor in isolated rat hepatocytes. Evidence for two potentially rate-limiting steps, J. Biol. Chem. 256 (6) (1981) 2615–2617.
[28] J.R. Lakowicz, Principles of Fluorescence Spectroscopy, third ed., Springer Science + Business Media, New York, USA, 2006.
[29] S. Vranic, N. Boggetto, V. Contremoulins, S. Mornet, N. Reinhardt, F. Marano, A. Baeza-Squiban, S. Boland, Deciphering the mechanisms of cellular uptake of engineered nanoparticles by accurate evaluation of internalization using imaging flow cytometry, Part. Fibre Toxicol. 10 (2013) 2.
[30] Y. Hu, J.M. Wan, A.C. Yu, Membrane perforation and recovery dynamics in microbubble-mediated sonoporation, Ultrasound Med. Biol. 39 (12) (2013) 2393–2405.
[31] S. Hernot, A.L. Klibanov, Microbubbles in ultrasound-triggered drug and gene delivery, Adv. Drug Deliv. Rev. 60 (10) (2008) 1153–1166.
[32] A.F. Lum, M.A. Borden, P.A. Dayton, D.E. Kruse, S.I. Simon, K.W. Ferrara, Ultrasound radiation force enables targeted deposition of model drug carriers loaded on microbubbles, J. Control. Release 111 (1–2) (2006) 128–134.
[33] S. Ibsen, G. Shi, C. Schutt, L. Shi, K.D. Suico, M. Benchimol, V. Serra, D. Simberg, M. Berns, S. Esener, The behavior of lipid debris left on cell surfaces from microbubble based ultrasound molecular imaging, Ultrasonics 54 (8) (2014) 2090–2098.
[34] O. Couture, M. Faivre, N. Pannacci, A. Babataheri, V. Servois, P. Tabeling, M. Tanter, Ultrasound internal tattooing, Med. Phys. 38 (2) (2011) 1116–1123.
[35] I. Lentacker, N. Wang, R.E. Vandenbroucke, J. Demeester, S.C. De Smedt, N.N. Sanders, Ultrasound exposure of lipoplex loaded microbubbles facilitates direct cytoplasmic entry of lipoplexes, Mol. Pharm. 6 (2) (2009) 457–467.
[36] P. Marmottant, M. Versluis, N. de Jong, S. Hilgenfeldt, D. Lohse, High-speed imaging of an ultrasound-driven bubble in contact with a wall: “Narcissus” effect and resolved acoustic streaming, Exp. Fluids 41 (2) (2005) 147–153.
[37] J. Collis, R. Manasseh, P. Liovic, P. Tho, A. Ooi, K. Petkovic-Duran, Y. Zhu, Cavitation microstreaming and stress fields created by microbubbles, Ultrasonics 50 (2) (2010) 273–279.
[38] C.E. Schutt, S.D. Ibsen, W. Thrift, S.C. Esener, The influence of distance between microbubbles on the fluid flow produced during ultrasound exposure, J. Acoust. Soc. Am. 136 (6) (2014) 3422.
[39] P.A. Dayton, J.S. Allen, K.W. Ferrara, The magnitude of radiation force on ultrasound contrast agents, J. Acoust. Soc. Am. 112 (5 Pt 1) (2012) 2183–2192.
[40] B. Geers, I. Lentacker, A. Alonso, N.N. Sanders, J. Demeester, S. Meairs, S.C. De Smedt, Elucidating the mechanisms behind sonoporation with adenovirus-loaded microbubbles, Mol. Pharm. 8 (6) (2011) 2244–2251.
[41] K.C. Partlow, G.M. Lanza, S.A. Wickline, Exploiting lipid raft transport with membrane targeted nanoparticles: a strategy for cytosolic drug delivery, Biomaterials 29 (23) (2008) 3367–3375.
[42] J.J. Lu, R. Langer, J. Chen, A novel mechanism is involved in cationic lipid-mediated functional siRNA delivery, Mol. Pharm. 6 (3) (2009) 763–771.
[43] K.C. Crowder, M.S. Hughes, J.N. Marsh, A.M. Barbieri, R.W. Fuhrhop, G.M. Lanza, S.A. Wickline, Sonic activation of molecularly-targeted nanoparticles accelerates transmembrane lipid delivery to cancer cells through contact-mediated mechanisms: implications for enhanced local drug delivery, Ultrasound Med. Biol. 31 (12) (2005) 1693–1700.
[44] Y. Luan, T. Faez, E. Gelderblom, I. Skachkov, B. Geers, I. Lentacker, T. van der Steen, M. Versluis, N. de Jong, Acoustical properties of individual liposome-loaded microbubbles, Ultrasound Med. Biol. 38 (12) (2012) 2174–2185.
[45] H. Chen, A.A. Brayman, W. Kreider, M.R. Bailey, T.J. Matula, Observations of translation and jetting of ultrasound-activated microbubbles in mesenteric microvessels, Ultrasound Med. Biol. 37 (12) (2011) 2139–2148.
[46] P. Dayton, A. Klibanov, G. Brandenburger, K. Ferrara, Acoustic radiation force in vivo: a mechanism to assist targeting of microbubbles, Ultrasound Med. Biol. 25 (8) (1999) 1195–1201.
[47] H. Chen, W. Kreider, A.A. Brayman, M.R. Bailey, T.J. Matula, Blood vessel deformations on microsecond time scales by ultrasonic cavitation, Phys. Rev. Lett. 106 (3) (2011) 34301.
[48] P. Prentice, A. Cuschieri, K. Dholakia, M. Prausnitz, P. Campbell, Membrane disruption by optically controlled microbubble cavitation, Nat. Phys. 1 (2005) 107–110.
[49] E. Unger, T. Porter, J. Lindner, P. Grayburn, Cardiovascular drug delivery with ultrasound and microbubbles, Adv. Drug Deliv. Rev. 72 (2014) 110–126.
[50] C.R. Mayer, R. Bekeredjian, Ultrasonic gene and drug delivery to the cardiovascular system, Adv. Drug Deliv. Rev. 60 (10) (2008) 1177–1192.
[51] H. Dewitte, S. Van Lint, C. Heirman, K. Thielemans, S.C. De Smedt, K. Breckpot, I. Lentacker, The potential of antigen and TriMix sonoporation using mRNA-loaded microbubbles for ultrasound-triggered cancer immunotherapy, J. Control. Release 194 (2014) 28–36.